

A Bayesian test for the appropriateness of a model in the biomagnetic inverse problem

R. Hasson* and S.J. Swithenby†,
The Open University,
Milton Keynes,
MK7 6AA
UK

June 19, 2021

Abstract

This paper extends the work of Clarke [1] on the Bayesian foundations of the biomagnetic inverse problem. It derives expressions for the expectation and variance of the *a posteriori* source current probability distribution given a prior source current probability distribution, a source space weight function and a data set. The calculation of the variance enables the construction of a Bayesian test for the appropriateness of any source model that is chosen as the *a priori* information. The test is illustrated using both simulated (multi-dipole) data and the results of a study of early latency processing of images of human faces.

Keywords

Biomagnetic inverse problem, Bayesian.

*Applied Mathematics department

†Physics department

1 Introduction

The magnetoencephalographic (MEG) inverse problem (sometimes known as the biomagnetic inverse problem) is the process of identifying the source current distribution inside the brain that gives rise to a given set of magnetic field measurements outside the head. The problem is difficult because the detectors are limited in number and are sensitive to widespread source currents, and because of the existence of silent and near-silent sources. 'Silent sources' are configurations of current density inside the brain which give zero magnetic field outside the head (e.g. all radial sources are silent when the head is modelled as a conducting sphere). It follows that the general biomagnetic inverse problem is ill-posed and under-determined.

The most common way of reducing the problem and rendering it tractable is by characterising the source in terms of a limited number of effective current dipoles. Such source descriptions provide links with the dominant functional architecture model of the brain in which processing is described in terms of localised activity with interactions between essentially separate regions. Multiple dipole models have enjoyed considerable success in the analysis of sensory and motor cortex (e.g. [2, 3, 4, 5]).

Growing evidence for the existence of more diffuse brain networks have led to an interest in distributed source algorithms. Several have been proposed [6, 7, 8, 9, 10, 11]. These algorithms have been designed to cope with the non-uniqueness of the problem, primarily by restriction of the source space and by regularisation. Each algorithm leads to a unique solution (from the infinite number available) through its particular choice of source basis, weight functions, noise assumptions, and, in many cases, cost function. There has been an extended debate about the accuracy and value of these methods. This proceeds at two levels; the technical ability of the various algorithms to recover a simulated source distribution (often quoted in terms of one or more source current dipoles), and the electrophysiological appropriateness of the type of source structure favoured by particular algorithm parameters. So, for example the simple minimum norm solution [7], which tends to produce a grossly smeared and superficial source distribution may be compared with the LORETA solution [10] which favours smooth but regionally confined current distributions. The issues have been fully debated in recent conferences [12, 13]).

The many to one nature of the mapping of sources to magnetic fields suggests that a probabilistic approach to reconstructing the sources from the magnetic field could be used. A Bayesian probabilistic approach was first proposed by Clarke [1]. More recently, Baillet et al have described an iterative approach which combines both spatial and temporal constraints within a unified Bayesian framework designed to allow the estimation of source activity that varies rapidly with position, e.g. across a sulcus [14]. Schmidt et al have developed a probabilistic algorithm in which a bridge is made between distributed and local source solutions through the use of a regional descriptor within the source representation [15]. In this case, a Monte Carlo method is used in the absence of an analytic solution for the expectation value of the source current.

Here, we are proposing an alternative Bayesian approach. It includes the explicit assumption of both a prior source current probability distribution and a source space weight function, and allows the calculation of the expectation and variance of the a-posteriori source current probability distribution. The derivation of these quantities is detailed in Section 3. The inclusion of the prior probability and the calculation of the variance provide a means by which the consistency of a model (assumed as the prior) can be tested against the data to reveal those parts of the source distribution that are statistically robust and, conversely, where the model is inadequate. Numerical calculation of significance is possible. A straightforward extension of this idea is the direct comparison of two data sets to reveal where, within a given model, there are significant differences in their associated source distributions. In the final part of this paper, both simulated and real data will be used to illustrate these various uses of the technique.

2 Specification of the problem

The arrangement of sources and detectors for the biomagnetic inverse problem is shown in Figure 1. The sources giving rise to the measurements are assumed to be restricted within a source space Q , which may be smaller than the whole head volume (e.g. if the sources are assumed to be cortical). The current density within the volume Q is assumed to belong to the space of square integrable vector fields on Q , which we call J .

The measurement process typically gives successive sets of data (~ 100 channels) every millisecond. In this paper the data for each time instant is processed independently, and the data from a single time instant

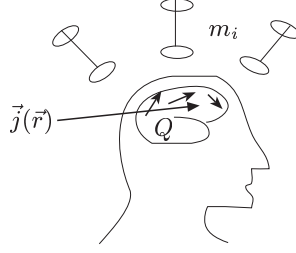


Figure 1: A schematic experimental geometry.

is collected into a vector $\tilde{m} \in \mathbb{R}^N$. If $\vec{j}(\vec{r}) \in J$ then the measurement process can be represented by a functional $z : J \rightarrow \mathbb{R}^N$. A subscript notation will be used to identify the sensor, i.e. z_i is the ideal reading from the i th sensor. So the basic equation is:

$$\tilde{m}_i = z_i(\vec{j}) + e_i \quad (1)$$

where the e_i are the measurement errors, which are assumed to be normally distributed with zero mean and covariance matrix $\alpha^2 D$ (where α is the standard deviation of the errors and D is a symmetric, positive definite matrix).

To compute the functional $z(\cdot)$ on a computer (i.e. to solve the forward problem) requires a volume conductor model of the head. In this paper the precise model used is irrelevant, so the final results will be written in terms of z . This is done via the Green's functions \vec{L}_i for the problem, which are defined by

$$z_i(\vec{j}) = \int_Q \vec{L}_i(\vec{r}) \cdot \vec{j}(\vec{r}) \, d\vec{r} \quad (2)$$

Stated simply, the inverse problem is to estimate $\vec{j}(\vec{r})$ given the data vector \tilde{m} . Obviously the given data are not enough to determine $\vec{j}(\vec{r})$ uniquely (for several reasons). The approach adopted here starts from the same point as used in Clarke [1], a statement of Bayes's theorem:

$$\mathcal{P}(\vec{j} \in A | m \in B) = \frac{\mathcal{P}(m \in B | \vec{j} \in A) \mathcal{P}(\vec{j} \in A)}{\mathcal{P}(m \in B)} \quad (3)$$

where A is a set of currents and B is a set of measurements. This equation reads, the *a posteriori* probability of a current set A after the measurement B is proportional to the probability of producing the measurement B given that the current is in the set A times the *a priori* probability of the current set A . ($\mathcal{P}(m \in B)$ is a constant for any measurement set B).

In this paper the probability distributions (both the prior probability and the errors) are assumed to be gaussian and so it is permissible to work with probability density functions. A further simplification is achieved by shrinking the measurement set B to a single point $\{\tilde{m}\}$ (this ignores the finiteness of the precision of the measurements). Equation 3 then becomes:

$$\rho_{\tilde{m}}(\vec{j}) \propto \rho(\vec{j}) \times \epsilon(\tilde{m} - z(\vec{j})) \quad (4)$$

where ρ is the *a priori* distribution, $\rho_{\tilde{m}}$ is the *a posteriori* distribution and ϵ is the error distribution. Throughout the paper, probability density functions will only be determined up to a constant. The constant of proportionality is found by requiring that the probability is normalised to one. In this paper both ρ and ϵ are assumed to be Gaussian and then $\rho_{\tilde{m}}$ is calculated to be Gaussian. An error probability density function ϵ consistent with the Gaussian assumption may be written:

$$\epsilon(e) \propto \exp \left\{ -\frac{1}{2\alpha^2} e^T D^{-1} e \right\} \quad (5)$$

This generally valid expression will be retained throughout the derivation in this paper. In practice, the noise covariance matrix D may be difficult to estimate and, for simplicity, the simple form $D = I$ will be used in the later illustrations.

3 Derivation

In this section formulae for the maximum likelihood current distribution and also the expected error distribution are derived under specific assumptions. First, an inner product on J is defined by:

$$\langle \vec{j}_1, \vec{j}_2 \rangle = \int_Q \frac{\vec{j}_1(\vec{r}) \cdot \vec{j}_2(\vec{r})}{\omega(\vec{r})} d\vec{r} \quad (6)$$

where $\omega(\vec{r})$ is a weighting distribution defined on the source space Q . This provides a method of inputting prior information of the location of sources (e.g. gained from MRI images) into the algorithm.

Clarke [1] assumed that the maximum likelihood prior current density was identically zero. Here that restriction is avoided and an arbitrary prior current \vec{j}^p will be introduced as a parameter of the method. The *a priori* probability distribution on J is defined using \vec{j}^p and the inner product:

$$\rho(\vec{j}) \propto \exp \left\{ -\frac{1}{2\beta^2} \langle \vec{j} - \vec{j}^p, \vec{j} - \vec{j}^p \rangle \right\} \quad (7)$$

where β is the assumed *a priori* standard deviation.

To proceed further a basis is needed for J . A ‘natural’ choice is a basis that is related to the measurement functional z . So an obvious candidate is a basis derived from the adjoint map to the measurement map from J to \mathbb{R}^N . This gives a map $\vec{z}: \mathbb{R}^N \rightarrow J$ (since J is self-dual) defined by:

$$\langle \vec{z}(a), \vec{j} \rangle = a^T z(\vec{j}) \quad (8)$$

Explicitly this gives the set of linearly independent distributions $\{\omega(\vec{r})\vec{L}_i(\vec{r})\}$. This set is extended into a basis of J that includes the silent sources by adding vectors $\{\vec{\mathcal{L}}_i\}$ which are chosen to be orthogonal to the $\{\omega\vec{L}_i\}$ i.e.

$$\langle \omega\vec{L}_i, \vec{\mathcal{L}}_j \rangle = 0 \quad \forall i, j \quad (9)$$

Since $\{\omega(\vec{r})\vec{L}_i\} \cup \{\vec{\mathcal{L}}_i\}$ is a basis of J a general current density $\vec{j}(\vec{r})$ can be written in terms of this basis as

$$\vec{j}(\vec{r}) = \sum_{i=1}^N a_i \omega(\vec{r})\vec{L}_i(\vec{r}) + \sum_i b_i \vec{\mathcal{L}}_i(\vec{r}) \quad (10)$$

To simplify the notation the components of currents are written in column vector notation:

$$\vec{j} = \begin{pmatrix} a \\ b \end{pmatrix}, \quad \vec{j}^p = \begin{pmatrix} a^p \\ b^p \end{pmatrix} \quad (11)$$

A simple computation gives

$$\langle \vec{j} - \vec{j}^p, \vec{j} - \vec{j}^p \rangle = \begin{pmatrix} a - a^p \\ b - b^p \end{pmatrix}^T \begin{pmatrix} P & 0 \\ 0 & Q \end{pmatrix} \begin{pmatrix} a - a^p \\ b - b^p \end{pmatrix} \quad (12)$$

where $P_{ij} = \langle \omega\vec{L}_i, \omega\vec{L}_j \rangle$ and $Q_{ij} = \langle \vec{\mathcal{L}}_i, \vec{\mathcal{L}}_j \rangle$ since by construction $\langle \omega\vec{L}_i, \vec{\mathcal{L}}_j \rangle = 0$.

Now the two *a priori* probability density functions (Equation 7 and Equation 5) may be combined with Bayes’s theorem (Equation 4) to obtain the *a posteriori* probability density:

$$\rho_{\tilde{m}}(\vec{j}) \propto \exp \left\{ -\frac{1}{2\beta^2} \begin{pmatrix} a - a^p \\ b - b^p \end{pmatrix}^T \begin{pmatrix} P & 0 \\ 0 & Q \end{pmatrix} \begin{pmatrix} a - a^p \\ b - b^p \end{pmatrix} \right\} \exp \left\{ -\frac{1}{2\alpha^2} (\tilde{m} - z(\vec{j}))^T D^{-1} (\tilde{m} - z(\vec{j})) \right\} \quad (13)$$

The task now is to manipulate this equation so that it is explicitly in the form of a gaussian distribution. As a first step the exponentials are combined:

$$\rho_{\tilde{m}}(\vec{j}) \propto \exp \left\{ -\frac{1}{2\alpha^2} \left[\begin{pmatrix} a - a^p \\ b - b^p \end{pmatrix}^T \begin{pmatrix} \zeta P & 0 \\ 0 & \zeta Q \end{pmatrix} \begin{pmatrix} a - a^p \\ b - b^p \end{pmatrix} + (\tilde{m} - Pa)^T D^{-1} (\tilde{m} - Pa) \right] \right\} \quad (14)$$

where $\zeta = \alpha^2/\beta^2$ and $z(\vec{j})$ has been replaced by Pa . Next, the terms involving operators on a are simplified by completing the square. All constant terms can be absorbed into the normalization constant of the probability density function and are ignored in this derivation.

$$\text{Operators on } a = (a - a^p)^\top \zeta P (a - a^p) + (\tilde{m} - Pa)^\top D^{-1} (\tilde{m} - Pa) \quad (15)$$

$$= a^\top \zeta P a - 2a^\top \zeta P a^p + a^\top P D^{-1} P a - 2a^\top P D^{-1} \tilde{m} + \text{const.} \quad (16)$$

$$= a^\top (\zeta P + P D^{-1} P) a - 2a^\top [P D^{-1} \tilde{m} + \zeta P a^p] + \text{const.} \quad (17)$$

$$= (a - \tilde{a})^\top (\zeta P + P D^{-1} P) (a - \tilde{a}) + \text{const.} \quad (18)$$

where \tilde{a} is defined by:

$$(\zeta P + P D^{-1} P) \tilde{a} = P D^{-1} \tilde{m} + \zeta P a^p \quad (19)$$

$$\text{So,} \quad \tilde{a} = (\zeta D + P)^{-1} (\tilde{m} + \zeta D a^p) \quad (20)$$

A modified expression for $\rho_{\tilde{m}}(\vec{j})$ is now available,

$$\rho_{\tilde{m}}(\vec{j}) \propto \exp \left\{ -\frac{1}{2\alpha^2} \begin{pmatrix} a - \tilde{a} \\ b - b^p \end{pmatrix}^\top \begin{pmatrix} P D^{-1} P + \zeta P & 0 \\ 0 & \zeta Q \end{pmatrix} \begin{pmatrix} a - \tilde{a} \\ b - b^p \end{pmatrix} \right\} \quad (21)$$

$$\propto \exp \left\{ -\frac{1}{2\alpha^2} \begin{pmatrix} a - \tilde{a} \\ b - b^p \end{pmatrix}^\top \begin{pmatrix} (P D^{-1} P + \zeta P)^{-1} & 0 \\ 0 & Q^{-1}/\zeta \end{pmatrix}^{-1} \begin{pmatrix} a - \tilde{a} \\ b - b^p \end{pmatrix} \right\} \quad (22)$$

This is explicitly in the form of a gaussian from which the mean current and covariance matrix can be identified by inspection. At this stage it is clear that the mean value of b is b^p i.e. that there is no change from our prior knowledge (this is because by construction all the information that the experiment provides is orthogonal to the $\vec{\mathcal{L}}_i$).

In order to produce images of the *a posteriori* current density, it is necessary to find the distribution of a single statistic that can be computed. The statistic is defined through a ‘test current’ $\vec{t} = \chi_{V_k}(\vec{r}) \hat{e}_\alpha$ where $\chi_{V_k}(\vec{r})$ is the characteristic function of a voxel in the brain and \hat{e}_α is a unit vector. This is another departure from Clarke [1] in which a delta function test current is assumed. This choice causes problems because the inner product $\langle \vec{t}, \vec{t} \rangle$ which is needed below (see Equation 46) is undefined for a delta function.

The distribution of the statistic $\lambda = \langle \vec{t}, \vec{j} \rangle$ will now be determined. First, the coefficients of the basis elements required to construct \vec{t} are identified:

$$\lambda = \langle \vec{t}, \vec{j} \rangle \quad (23)$$

$$= \left\langle \vec{t}, \sum_i a_i \omega(\vec{r}) \vec{\mathcal{L}}_i(\vec{r}) + \sum_i b_i \vec{\mathcal{L}}_i(\vec{r}) \right\rangle \quad (24)$$

$$= \sum_i a_i \langle \vec{t}, \omega(\vec{r}) \vec{\mathcal{L}}_i(\vec{r}) \rangle + \sum_i b_i \langle \vec{t}, \vec{\mathcal{L}}_i(\vec{r}) \rangle \quad (25)$$

$$= u^\top a + v^\top b, \text{ say.} \quad (26)$$

Equation 22 is projected onto this particular linear combination of co-ordinates to find the probability density of λ

$$\rho_{\tilde{m}}(\lambda) \propto \exp \left\{ -\frac{1}{2\alpha^2} \frac{(u^\top a + v^\top b - u^\top \tilde{a} - v^\top b^p)^2}{u^\top (P D^{-1} P + \zeta P)^{-1} u + v^\top Q^{-1} v / \zeta} \right\} \quad (27)$$

The mean of λ can be identified from Equation 27 by inspection.

$$\text{mean of } \lambda = u^\top \tilde{a} + v^\top b^p \quad (28)$$

The term $v^T b^p$ cannot be computed directly since the basis fields $\vec{\mathcal{L}}_i$ have not been defined explicitly. The problem may be overcome by expanding $\langle \vec{t}, \vec{j}^p \rangle$

$$\langle \vec{t}, \vec{j}^p \rangle = \left\langle \vec{t}, \sum_i a_i^p \omega(\vec{r}) \vec{L}_i(\vec{r}) + \sum_i b_i^p \vec{\mathcal{L}}_i(\vec{r}) \right\rangle \quad (29)$$

$$= \sum_i a_i^p \langle \vec{t}, \omega(\vec{r}) \vec{L}_i(\vec{r}) \rangle + \sum_i b_i^p \langle \vec{t}, \vec{\mathcal{L}}_i(\vec{r}) \rangle \quad (30)$$

$$= u^T a^p + v^T b^p \quad (31)$$

Equation 28 may now be rewritten using only references to known vector fields as:

$$\text{mean of } \lambda = u^T \tilde{a} + \langle \vec{t}, \vec{j}^p \rangle - u^T a^p \quad (32)$$

$$= u^T (\zeta D + P)^{-1} (\tilde{m} + \zeta D a^p) + \langle \vec{t}, \vec{j}^p \rangle - u^T a^p \quad (33)$$

$$= u^T (\zeta D + P)^{-1} (\tilde{m} - P a^p) + \langle \vec{t}, \vec{j}^p \rangle \quad (34)$$

This equation explicitly writes the expectation value of the statistic $\lambda = \langle \vec{t}, \vec{j} \rangle$ as a sum of two terms. The second term is the statistic for the prior current, and so the first term can be identified as the correction to the prior suggested by the measurements i.e. the first term shows the difference between the expectation of $\langle \vec{t}, \vec{j} \rangle$ before and after the experiment was made. This is the first central result of this paper and it is worth stating explicitly:

$$\text{Change in expectation of } \langle \vec{t}, \vec{j} \rangle = u^T (\zeta D + P)^{-1} (\tilde{m} - z(\vec{j}^p)) \quad (35)$$

Using Equation 27 it is possible to go further than this and determine the statistical significance of the statistic. This is because the variance of the variable λ can also be read off from Equation 27 as:

$$\text{variance of } \lambda = \alpha^2 \left[u^T (P D^{-1} P + \zeta P)^{-1} u + \frac{1}{\zeta} v^T Q^{-1} v \right] \quad (36)$$

In order to derive an expression in the form of computable matrices, the term $v^T Q^{-1} v$ must be rewritten. To do so, \vec{t} is written as a linear combination of basis elements:

$$\vec{t}(\vec{r}) = \sum_i x_i \omega(\vec{r}) \vec{L}_i(\vec{r}) + \sum_i y_i \vec{\mathcal{L}}_i(\vec{r}) \quad (37)$$

Of course x and y are related to u and v . In fact:

$$u_i = \langle \vec{t}, \omega(\vec{r}) \vec{L}_i(\vec{r}) \rangle \quad (38)$$

$$= \left\langle \sum_j x_j \omega(\vec{r}) \vec{L}_j(\vec{r}) + \sum_j y_j \vec{\mathcal{L}}_j(\vec{r}), \omega(\vec{r}) \vec{L}_i(\vec{r}) \right\rangle \quad (39)$$

$$= \sum_j x_j \langle \omega(\vec{r}) \vec{L}_j(\vec{r}), \omega(\vec{r}) \vec{L}_i(\vec{r}) \rangle \quad (40)$$

$$= \sum_j x_j P_{ij} \quad (41)$$

Similarly, $v = Qy$. Using these relationships, the inner product of \vec{t} with itself can be computed:

$$\langle \vec{t}, \vec{t} \rangle = \left\langle \sum_i x_i \omega(\vec{r}) \vec{L}_i(\vec{r}) + \sum_i y_i \vec{\mathcal{L}}_i(\vec{r}), \sum_j x_j \omega(\vec{r}) \vec{L}_j(\vec{r}) + \sum_j y_j \vec{\mathcal{L}}_j(\vec{r}) \right\rangle \quad (42)$$

$$= x^T P x + y^T Q y \quad (43)$$

$$(44)$$

from which,

$$\langle \vec{t}, \vec{t} \rangle = u^T P^{-1} u + v^T Q^{-1} v \quad (45)$$

Equations 36 and 45 can now be combined to generate the following formula for the variance:

$$\text{variance of } \lambda = \alpha^2 \left[u^T (PD^{-1}P + \zeta P)^{-1} u + \frac{1}{\zeta} (\langle \vec{t}, \vec{t} \rangle - u^T P^{-1} u) \right] \quad (46)$$

This equation is a generalisation of the results of Clarke [1], some consequences of it were explored in [16] and [17]. It is interesting to note that the existence of a prior current density does not affect this variance.

It may be helpful to relate features of this equation to the measurement system. The second term in Equation 46 is multiplied by $\alpha^2/\zeta = \beta^2$ and so is independent of the assumed noise levels in the detectors. It represents a variance derived from the finite number of measurements and the geometry of the experiment. Since it is proportional to β^2 , it can be interpreted in terms of the truncation error becoming less and less important as the certainty of the prior distribution \vec{j}^p increases.

The first term in Equation 46 is proportional to α^2 . It shows how the noise in the data is reflected into source space. The unregularised form of this term was derived previously by Ioannides et al in [18] using an *ad hoc* argument. Ioannides et al obtained the regularised form by replacing occurrences of P^{-1} in the unregularised form by $(P + \zeta I)^{-1}$. In the notation used here this gives a first term as follows

$$\text{first term} = u^T (P + \zeta I)^{-1} (P + \zeta I)^{-1} u \quad (47)$$

This does not agree with Equation 46 which has the form (in the case of the measurement error being uncorrelated, i.e. $D = I$)

$$\text{first term} = u^T P^{-1} (P + \zeta I)^{-1} u \quad (48)$$

The behaviour as ζ tends to infinity is that the variance tends to zero. This is reasonable since, for fixed experimental noise levels (i.e. fixed α), ζ tending to infinity corresponds to β tending to zero, which in turn corresponds to greater and greater certainty that the prior is correct. When β is zero the *a priori* current distribution is known with absolute certainty. This is consistent with the above analysis which indicates that, in this case, the *a posteriori* current density is certain to be equal to the *a priori* current density.

Note that, when computing the term $u^T P^{-1} u$ in Equation 46, any reasonable algorithm (e.g. Choleski's algorithm) for computing $P^{-1} u$ can be used even though the matrix P is ill-conditioned. This is because the large residual vector which results in this calculation is annihilated by the inner product with u . So the computation of the whole term is well conditioned.

4 Applications

The main analytical results of this paper (Equations 34, 35 and 46) provide the means of solving the MEG inverse problem with specific assumptions and of assessing the robustness of the solution. In this section, this approach will be illustrated through three studies: a simulation of a few-dipole source set; an analysis of the appropriate dipole model for data from a real experiment on face processing; and a comparison of responses to different visual stimuli from the same real experiment.

All the illustrations are based on the same experimental arrangement and the same instrument, the Neuromag-122TM [19]. This is a helmet MEG system that contains 61 pairs of first order gradiometers ($\partial B_r/\partial\theta$, $\partial B_r/\partial\phi$ in spherical polar co-ordinates), covering the head (Figure 2). The outputs of each pair of detectors are closely related to the dominant tangential ionic current flow in the region underlying the relevant sensors. Also shown in Figure 2 is the assumed source space, a 2-d spherical shell of radius 0.08 m covering a 2 radian by 2 radian solid angle over posterior regions of the cortex.

The source configuration for the first simulation study was three dipoles distributed in an isosceles triangle configuration (co-ordinates (0,-0.08m,-0.02m), (-0.05m,-0.06m,0.02m) and (0.05m,-0.06m,0.02m) with orientations (1,0,1), (1,0,-1), (1,0,1) respectively). The positions of the dipoles were chosen so as to represent approximately a central primary and two bilateral secondary visual processing areas. The precise

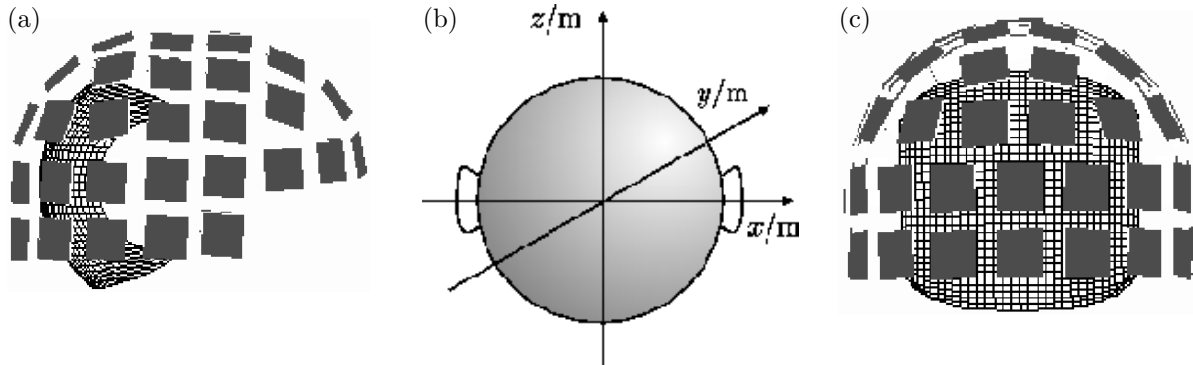


Figure 2: The experimental geometry. a) and c) show the 61 measurement sites in the helmet arrangement. Each square represents a pair of orthogonal detectors. Also shown is the source space, consisting of a discretised mesh covering a part of a spherical shell. b) Shows the coordinate system with the x-axis along the line joining the pre-auricular points and the y-axis joining theinion and nasion.

locations are not exactly on the source space shell but are displaced by 3 mm, 1 mm, and 1 mm respectively from the shell. The dipole locations and activation curves are shown in Figure 3. The central source is activated first, followed by synchronous activation of the lateral sources. The forward problem is solved using a homogeneous sphere conductor model centred at the origin. Gaussian noise has been added to the computed dipole signal so that the integrated noise power is equal to 50% of the integrated signal power. Examples of simulated data are shown in Figure 3c.

The simplest approach to the inverse problem is to use Equation 34 with a zero prior current distribution. This simplification results in the same formulae as the probabilistic algorithm that has been used for several years [20, 21]. The resulting expectation of the *a-posteriori* current distribution is shown in Figure 4a.

However, using our analysis, it is possible to employ an approach which goes further in comparing different source descriptions. Single or few dipole solutions can be generated from the magnetic field data and used as prior estimates of the current distribution. It is then possible to identify the appropriateness of this particular dipole-model prior estimate by computing from Equation 35 the change in the expectation associated with including the measurement information without constraining the final solution to a dipolar form. Because the statistic provides spatial information it indicates directly those areas where the dipole model solution has been modified. Using the variance associated with the *a-posteriori* current (computed from Equation 46) allows us to plot the number of standard deviations of the change in expectation at each point in source space.

To illustrate the usefulness of this technique, two prior descriptions of the source current for this data are postulated - a single moving dipole model and a two moving dipole model. The optimal solutions have been found through exhaustive search of the discretised source space by least squares minimisation of the fit to the data. The positions of the fitted dipoles for nine time slices are shown in Figure 4b. They may be compared with the nearest points on the source space to the actual dipole positions. Using each model in turn as a prior current and Equations 35 and 46, the statistical significance of the differences between the *a-posteriori* and the *a-priori* current distributions are calculated (Figure 4b).

It can be seen that a single dipole is a good model for the first two time instants and also for the ninth. This is not surprising as only one dipole is active at these times. The significance plots for the other times suggest systematic discrepancies between the model and the data. The restricted localisation of these significant differences points to additional localised sources that have been omitted from the model. The next step is the two dipole model (Figure 4c). The two-dipole significant difference diagram suggests that this model is adequate for all but four time instants. Comparison with the activation curves identifies these as being the times when all three dipoles are active.

The second illustration uses data from an evoked response study of face-processing using the same experimental system [23]. Human subjects were presented briefly with photographs of human faces and control

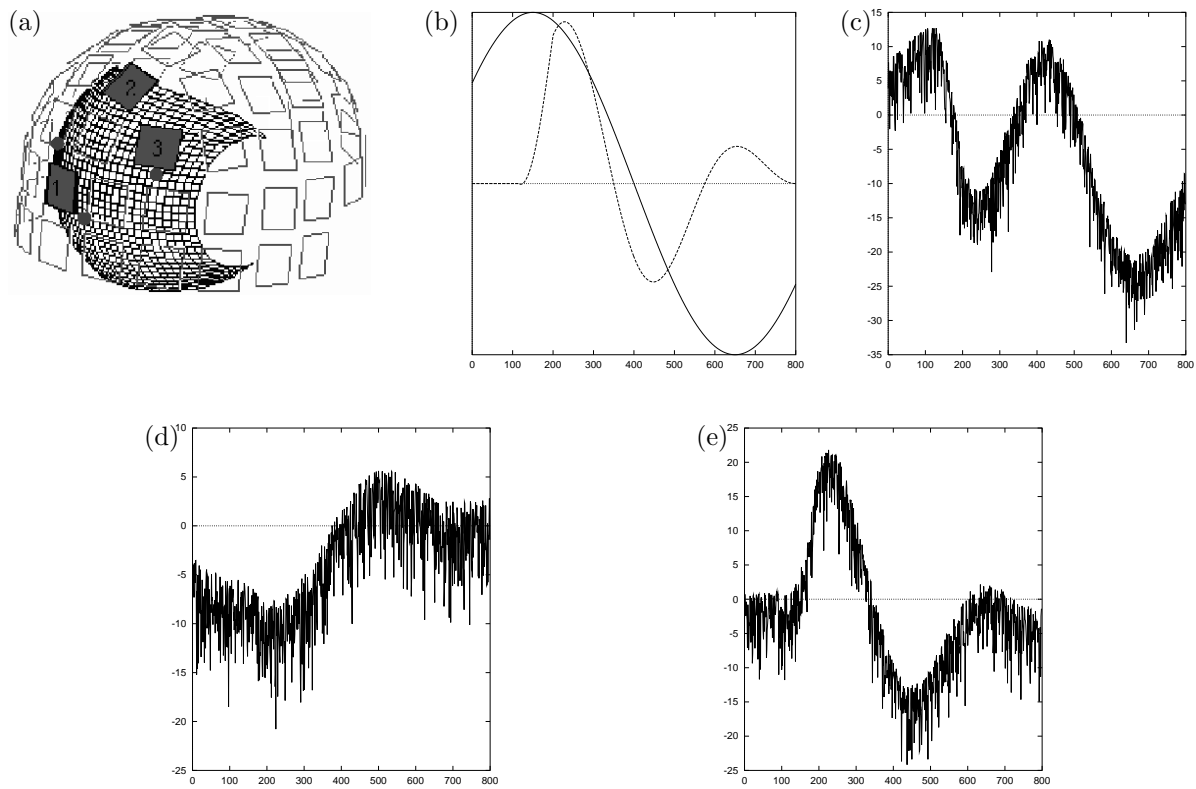


Figure 3: a) An isometric projection of the experimental geometry. The dots on the source space are the feet of the perpendiculars from the three dipole sources used in this simulation. The activation curves (dipole moment vs. time in milliseconds) for these three dipoles are shown in b). The longer period curve corresponds to the dominant (central) source. The other curve corresponds to the synchronous and equally activated lateral sources. The highlighted detector sites are those for which the data is shown in c) channel 1 d) channel 2 and e) channel 3. Note that it is only in the case of Channel 3 that the signal follows clearly the activation curve for the closest dipole.

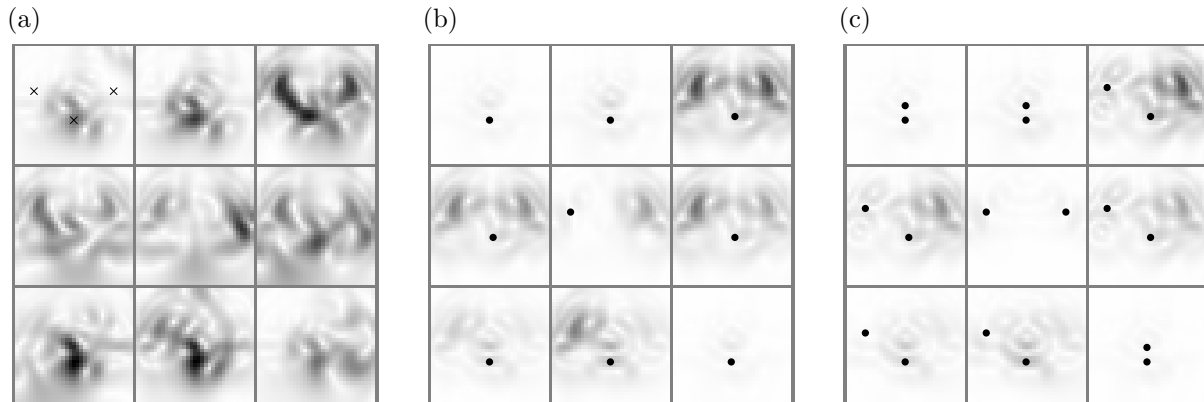


Figure 4: (a) The maximum likelihood current density with a zero *a priori* current distribution. Each frame is a two dimensional representation of the shell source space pictured in Figure 2. The 9 frames are snapshots at time 0 ms, 100 ms, 200 ms, etc. (see Figure 3). They should be read left to right and top to bottom. The optimal regularization parameter was determined by the L-curve method [22] to be $0.283 \times \text{trace}(P)/N$. The crosses on the first frame of this sequence show the positions of the three source dipoles in this representation of the source space. (b) The significant differences between a single moving dipole model and the computed data. The black dots denote the projected position of the fitted dipole. (c) As (b) but with a two moving dipole model.

objects (e.g. animals) and their neural responses were recorded as a function of time after the stimulus. It is known that the early response to face images involves widespread activity in the posterior brain but there is limited evidence for the precise distribution and timecourse of the neuronal sources. One suggestion is that there are three major areas of activity; in occipital cortex and both right and left ventral occipito-temporal cortex [24, 25]. Strong occipital activity (starting about 100 ms after the stimulus) is expected to lead to concurrent activity in the two other regions with a stronger response in the right hemisphere [23]. The hypothesised arrangement is therefore similar in geometry to the simulated measurement already discussed.

Figure 5 shows the same set of outputs that were presented for the simulated system. In this case, the fitted dipoles may be thought of as representing a discrete limited region of source current. Figure 5a suggests early central activity (frame 3) followed by less prominent localised activity on the right (frame 5). These source regions are reflected in the 1-dipole solutions (Figure 5b). However, comparison with Figure 3b shows that the accuracy of the single dipole fit is less than for the simulated data even though the noise levels are comparable. This may suggest that there are other active sources present. There is no evidence that these are recovered by the 2-dipole model (Figure 5c) as there is little improvement in the significant difference maps generated using a two dipole model as the prior (see for example the strong similarity between frame 4 in Figures 5b and 5c). It would be reasonable to infer that the additional sources are diffuse.

The third illustration relates to the main thrust of the face processing study by Swithenby et al [23], which was to identify statistically significant evidence for differences between the responses to faces and the other complex visual stimuli. In the initial analysis the strength of evoked activity within a certain region and latency span was parameterised in terms of the signal power integrated over a group of channels and a specified latency span. These calculations revealed that the brain activity in the right occipito-temporal region following face presentation is significantly different ($p=0.05$) from activity following non face images during the latency span 110 to 170 ms. No other consistent and statistically significant differences were found. This data-space analysis, though useful, was complicated by the need to survey the large number of possible choices of channel group and latency range.

The Bayesian framework developed here provides an alternative direct means of directly comparing responses to two stimuli. By using one data set as the prior and comparing it with the other data set it is possible to identify those regions in source space where there is a statistically significant difference between the two source structures within the same source model. We have carried out this calculation for the face and control stimuli as a function of position and latency for a simple two-dimensional source space consisting of a part spherical shell whose radius is similar to that of the cortical surface (Figure 6).

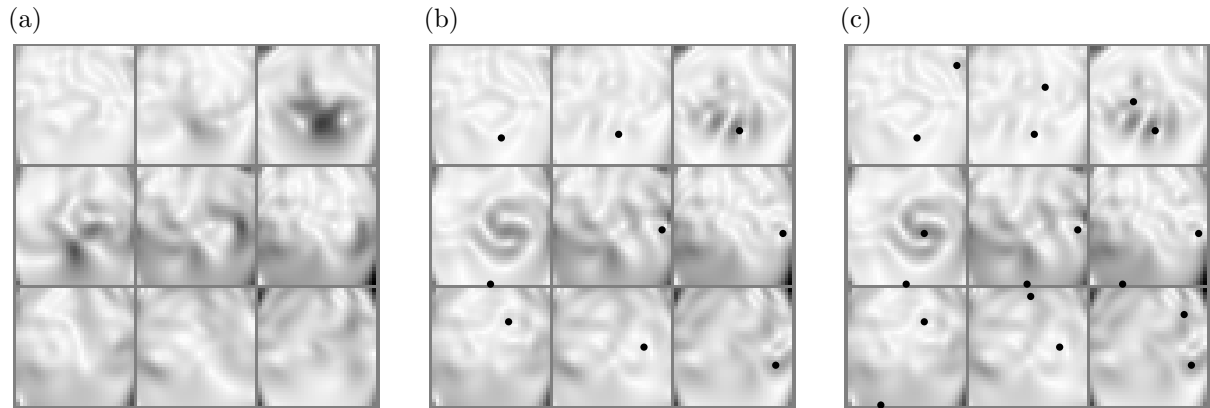


Figure 5: (a) The maximum likelihood current density for the face response with a zero *a priori* current distribution. The 9 frames represent equal steps in time from 70 ms to 241 ms after the stimulus. (b) The significant differences between a single moving dipole model and the computed data. The black dots denote the projected positions of a single dipole. (c) As (b) but with a two moving dipole model.

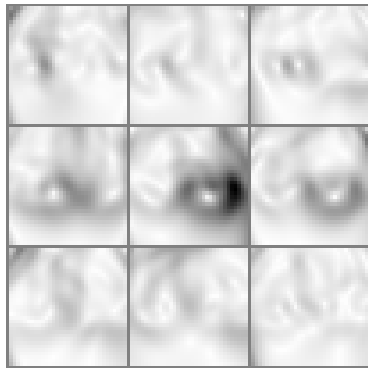


Figure 6: The maximum likelihood current density for the face response with a *a priori* current distribution derived from the control experiment with pictures of animals. The 9 frames represent equal steps in time from 70 ms to 241 ms after the stimulus. The regularisation parameter ζ was chosen by using the L-curve method [22]. The optimal value was $1.4 \times \text{trace}(P)/N$.

The evidence for statistically significant differences in the right occipito-temporal region at about 155 ms is clear. However there is no evidence for differences in earlier latencies, in particular with respect to the early source shown in Figure 5a.

5 Discussion

The illustrations provided above offer ways of exploiting the new Bayesian results that have been derived. Dipole predictions have been systematically examined using a measure that goes beyond a simple scalar goodness of fit measure (i.e. percentage of variance accounted for) to a statistically valid map of fitting significance. This addresses a long standing issue, the unreliability of the goodness of fit measure as a reliable test of the appropriateness of a given model in explaining a given set of data [26]. The spatially discriminated Bayesian approach gives a test which is more reliable when there is fundamental concern about the appropriateness of a model. The second example shows how these ideas may be applied to real data to assess the complexity of the dipole model that a given data set can sustain. In similar fashion, the third example illustrates how the Bayesian framework allows the direct comparison of two data sets in order to identify quantitatively the regions of statistically significant source activities.

These ideas may be extended further within MEG (and EEG) data analysis. An obvious extension is to perform dipole analysis as a precursor to a distributed Bayesian analysis. This may provide a way of not only refining information about the depth of source activity but also of assessing the reliability of depth estimates. Other possibilities include exploration of the dynamics. For example, times at which there are statistically significant change in the data could be identified by using a source distribution estimated from each time as the prior for an analysis of the data from the next sampling instant.

In summary, the analysis presented here comprises a Bayesian estimator of a source current distribution in the biomagnetic inverse problem. This is generalisable to other systems and may be used as the engine for tests of significant difference in source models and data.

References

- [1] C.J.S. Clarke. Error estimates in the biomagnetic inverse problem. *Inverse Problems*, 10:77–86, 1994.
- [2] S. Vanni, B. Rockstroh, and R. Hari. Cortical sources of human short-latency somatosensory evoked fields to median and ulnar nerve stimuli. *Brain Research*, 737:25–33, 1996.
- [3] H. Buchner, L. Adams, A. Muller, I. Ludwig, A. Knepper, A. Thron, K. Niemann, and M. Scherg. Somatotopy of human hand somatosensory-evoked potentials and 3D-NMR tomography. *Electroenceph. clin. Neurophys.*, 96(2):121–134, 1995.
- [4] F. Mauguiere, I. Merlet, N. Forss, S. Vanni, V. Jousmaki, P. Adeleine, and R. Hari. Activation of a distributed somatosensory cortical network in the human brain. a dipole modelling study of magnetic fields evoked by median nerve stimulation. 1. location and activation timing of sef sources. *Electroenceph. clin. Neurophys.*, 104(4):281–289, 1997.
- [5] M. Hoshiyama, R. Kakigi, S. Koyama, S. Watanabe, and M. Shimojo. Activity in posterior parietal cortex following somatosensory stimulation in man: Magnetoencephalographic study using spatio-temporal source analysis. *Brain Topography*, 10(1):23–30, 1997.
- [6] M.S. Hämäläinen and R.J. Ilmoniemi. Interpreting measured magnetic fields of the brain: Estimates of current distributions. Technical Report TKK-F-A559, Helsinki University of Technology, 1984.
- [7] M.S. Hämäläinen and R.J. Ilmoniemi. Interpreting magnetic fields of the brain: minimum norm estimates. *Med. & Biol. Eng. & Comput.*, 32:35–42, 1994.
- [8] A.A. Ioannides, J.P.R. Bolton, R. Hasson, and C.J.S. Clarke. Localised and distributed source solutions for the biomagnetic inverse problem II. In S.J. Williamson, M. Hoke, G. Stroink, and M. Kotani, editors, *Advances in Biomagnetism*, pages 591–595, New York, August 1989. Plenum Press.

- [9] J.Z. Wang, S.J. Williamson, and L. Kaufman. Magnetic source images determined by a lead-field analysis - the unique minimum-norm least-squares estimation. *IEEE Transactions on Biomedical Engineering*, 39:665–675, 1992.
- [10] R.D. Pascual-Marqui. Low resolution brain electromagnetic tomography. *Brain Topography*, 7:180, 1994.
- [11] I.F. Gorodnitsky, J.S. George, and B.D. Rao. Neuromagnetic source imaging with focuss: a recursive weighted minimum norm algorithm. *Electroenceph. clin. Neurophys.*, 95:231–251, 1995.
- [12] W. Skrandies (Ed.). Extended discussion of LORETA. *International Society for Brain Electromagnetic Topography Newsletter*, 6, ISSN 0947-5133, December 1995.
- [13] C. Wood (ed.). Workshop on the meg inverse problem. In *Advances in Biomagnetism Research: Biomag96*, (Eds: C. Aine et al) Springer-Verlag, New York, In press, 1998.
- [14] S. Baillet and L. Garnero. A Bayesian approach to introducing anatomo-functional priors in the EEG/MEG inverse problem. *IEEE Trans. Biomed. Eng.*, 44(5):374–385, 1997.
- [15] D. M. Schmidt, J.S. George, and C.C. Wood. Bayesian inference applied to the electromagnetic inverse problem. Preprint la-ur-97-4813, Los Alamos National Laboratory, 1997.
- [16] R. Hasson and S.J. Swithenby. A quantitative analysis of the EEG and MEG inverse problems. In C. Baumgartner, L. Deecke, G. Stroink, and S.J. Williamson, editors, *BIOMAGNETISM: Fundamental research and clinical applications*, pages 455–457, Amsterdam, August 1993. Elsevier Science.
- [17] R. Hasson and S. J. Swithenby. Aspects of non-uniqueness: how one source affects the reconstruction of another. In *Advances in Biomagnetism Research: Biomag96*, (Eds: C. Aine et al) Springer-Verlag, New York, In press, 1998.
- [18] A.A. Ioannides, J.P.R. Bolton, and C.J.S. Clarke. Continuous probabilistic solutions to the biomagnetic inverse problem. *Inverse Problems*, 6:523–542, 1990.
- [19] J.E.T. Knuutila, A.I. Ahonen, M.S. Hämäläinen, M.J. Kajola, P.P. Laine, O.V. Lounasmaa, L.T. Parkkonene, J.T.A Simola, and C.D. Tesche. A 122-channel whole cortex SQUID system for measuring the brain’s magnetic field. *IEEE Trans. Mag.*, 29 (6):3315–3320, 1993.
- [20] C.J.S. Clarke. Probabilistic modelling of continuous current sources. In J.Nenonen, H.-M.Rajala, and T.Katila, editors, *Biomagnetic Localisation and 3D modelling*, pages 117–125, Helsinki, May 1991. Helsinki University of Technology, Dept. of Technical Physics.
- [21] C.J.S. Clarke and B.S. Janday. The solution of the biomagnetic inverse problem by maximum statistical entropy. *Inverse Problems*, 5:483–500, 1989.
- [22] P.C. Hansen. Regularization tools. *Numerical Algorithms*, 6:1–35, 1994.
- [23] S.J. Swithenby, A.J. Bailey, S. Bräutigam, O.E. Josephs, V. Jousmäki, and C.D.Tesche. Neural processing of human faces: a magnetoencephalographic MEG study. *Expt. Brain Res.*, 118:501–510, 1998.
- [24] S.T. Lu, M.S. Hämäläinen, R. Hari, R.J. Ilmoniemi, O.V. Lounasmaa, M. Sams, and V. Vilkmán. Seeing faces activates three separate areas outside the occipital visual cortex in man. *Neuroscience*, 43 (2/3):287–290, 1991.
- [25] E. Halgren, T. Raij, K. Marinkovic, V. Jousmaki, and R. Hari. Magnetic fields evoked by faces in the human brain: 1. topography and equivalent dipole locations. *Society for Neuroscience*, 21:562, 1995.
- [26] B.S. Janday and S.J. Swithenby. The use of the symmetric sphere model in magnetoencephalographic analysis. In S.N. Erne and G.L. Romani, editors, *Advances in Biomagnetism Functional Localization: A challenge for Biomagnetism*, pages 153–160, London, 1989. World Scientific.